

---

# Maximum Causal Entropy Inverse Constrained Reinforcement Learning

---

Mattijs Baert<sup>\*1,2</sup> Pietro Mazzaglia<sup>1,2</sup> Sam Leroux<sup>1,2</sup> Pieter Simoons<sup>1,2</sup>

## Abstract

When deploying artificial agents in real-world environments where they interact with humans, it is crucial that their behavior is aligned with the values, social norms or other requirements of that environment. However, many environments have implicit constraints that are difficult to specify and transfer to a learning agent. To address this challenge, we propose a novel method that utilizes the principle of maximum causal entropy to learn constraints and an optimal policy that adheres to these constraints, using demonstrations of agents that abide by the constraints. We prove convergence in a tabular setting and provide an approximation which scales to complex environments. We evaluate the effectiveness of the learned policy by assessing the reward received and the number of constraint violations, and we evaluate the learned cost function based on its transferability to other agents. Our method has been shown to outperform state-of-the-art approaches across a variety of tasks and environments, and it is able to handle problems with stochastic dynamics and a continuous state-action space.

## 1. Introduction

The behavior of individuals in today’s society is shaped by social norms, which provide predictability, safety and efficiency in human interaction. Similarly, successful integration of artificial agents in the real-world requires *value alignment* of their behavioral policies (Christian, 2020; Balakrishnan et al., 2019; Russell, 2019). As an example, a self-driving car should not only efficiently transport its passengers to their destination, but it should also adhere to traffic regulations, such as traffic signs, traffic lights, and road conditions, to ensure the safety of all road users. Furthermore it is essential to program social norms into the agent prior to deployment to ensure that rule violations are

avoided at all times. Learning value-aligned policies can be viewed as optimizing an objective subject to a set of constraints. In the framework of Reinforcement Learning (RL) this entails finding a policy that maximizes a combination of objectives, i.e. the goal of the task and the constraints, where each objective is weighted according to its importance. Not only does each combination of weights lead to a different Pareto optimal solution (Van Moffaert & Nowé, 2014), also tuning these coefficients is a difficult and time-consuming process, as the task goal and the social norms often conflict with one another (Mania et al., 2018). An alternative approach for solving the constrained RL problem is by utilizing a primal-dual method to learn the optimal coefficients (Bhatnagar & Lakshmanan, 2012; Tessler et al., 2018). Although it is straightforward to define constraints for simple environments, this is not the case for real-world settings, which often comprise multiple and implicit constraints. Returning to the traffic example, human drivers also adopt implicit rules, for example driving slower when traffic is heavy or leaving more space when driving behind a truck. We propose to solve this problem by learning a cost function that embodies the constraints of the environment from demonstrations of constraint-abiding agents.

Recent advancements in Inverse Reinforcement Learning (IRL) have enabled learning a reward function from expert demonstrations in challenging environments (Ho & Ermon, 2016; Finn et al., 2016; Fu et al., 2017). However, there are relatively few studies that focus on learning a cost function, also known as Inverse Constrained Reinforcement Learning (ICRL). Although IRL and ICRL seem very related, there is a main difference in how they handle states which do not occur during the expert demonstrations. The states which are not visited by the expert can be subdivided into a group of constrained states and a group of states which are unconstrained but correspond with low rewards. IRL does not distinguish these two groups of unvisited states which could cause constraint violations when the agent ends up in states which were never visited by the expert. ICRL, on the other hand, explicitly distinguishes these two groups by assigning high costs to constrained states.

Various ICRL approaches use the principle of maximum entropy to learn a set of constraints that conform to expert data while remaining as unbiased as possible (Scobee & Sastry, 2019; Stocking et al., 2021; Glazier et al., 2022). This work has been extended to domains with unknown

<sup>1</sup>IDLab, Department of Information Technology at Ghent University <sup>2</sup>imec. Correspondence to: Mattijs Baert <mat-tijs.baert@ugent.be>.

transition dynamics and continuous state-action spaces (Mallik et al., 2021; Liu et al., 2022). The principle of maximum (non-causal) entropy holds true only for environments with deterministic transition dynamics. To learn constraints in stochastic environments, McPherson et al. (2021) proposed a method based on the principle of maximum causal entropy. However, this algorithm’s running time increases cubically with the size of the state space, making it unable to scale to continuous state-action spaces. This limitation also applies to methods based on Bayesian theory (Papadimitriou et al., 2021), which define the set of constraints as a collection of discrete states.

Our main contribution is an ICRL method that, to the best of our knowledge, is the first to scale to environments with a continuous state-action space and stochastic dynamics. We formulate a new ICRL objective drawing from feature expectation matching (Abbeel & Ng, 2004) and in contrast to most previous work, from the principle of maximum causal entropy (Ziebart et al., 2010) instead of the principle of maximum (non-causal) entropy (Ziebart et al., 2008). From this objective, we derive two algorithms to learn both a cost function, representing constraints, and a policy that adheres to the learned constraints. First, we propose an algorithm based on policy iteration and present proof of its convergence. Next, we introduce an approximation of the first method that can be implemented using deep neural networks and scales to problems with a continuous state-action space. We evaluate the performance of the learned policy by measuring the received reward and the number of constraint violations in both virtual and realistic environments. Next, we evaluate the learned cost function on its transferability to different types of agents with other reward functions. Finally, we examine the importance of different parts of the proposed method through an ablation study. Based on our empirical evaluation, we have found that our method surpasses the performance of state-of-the-art techniques.

The structure of the paper is as follows: In Section 2, we present the necessary background information on constrained Markov decision processes and inverse reinforcement learning. Our proposed method is outlined in Section 3. We evaluate and compare the results of our method to existing state-of-the-art approaches in Section 4. In Section 5, we discuss related work. Finally, we conclude and provide future directions in Section 6.

## 2. Background

### 2.1. Constrained Markov Decision Process

A Markov decision process (MDP) is defined by a state space  $\mathcal{S}$ , an action space  $\mathcal{A}$ , a discount factor  $\gamma \in [0, 1]$ , a transition distribution  $p(s' | s, a)$  which specifies the probability of transitioning to state  $s'$  when performing action  $a$  while in state  $s$ , an initial state distribution  $\mathcal{I}(s)$  and

a bounded reward function  $R : \mathcal{S} \times \mathcal{A} \mapsto [r_{\min}, r_{\max}]$  specifying the scalar reward the agent receives for applying action  $a$  while in state  $s$ . We consider an agent interacting with the environment at discrete timesteps  $t$  generating a sequence of transitions called a trajectory  $\tau = ((s_0, a_0, s_1), \dots, (s_{T-1}, a_{T-1}, s_T))$  of length  $T$ . We define the reward of a trajectory as the sum of discounted rewards:  $R(\tau) = \sum_{t=0}^{T-1} \gamma^t R(s_t, a_t)$ . At every timestep, the agent selects its action based on a policy  $\pi : \mathcal{S} \mapsto \mathcal{P}(\mathcal{A})$  which is a mapping from a state to a probability distribution over actions. The goal of forward reinforcement learning is to find the policy which maximizes the expected sum of discounted rewards:  $\max_{\pi} \mathbb{E}_{\tau \sim \pi} R(\tau)$ .

A constrained Markov decision process (CMDP)  $\mathcal{M}^C$  (Altman, 1999) is defined as an MDP augmented with a non-negative bounded cost function  $C : \mathcal{S} \times \mathcal{A} \mapsto [c_{\min}, c_{\max}]$  and a budget  $\alpha \geq 0$ .  $C(s, a)$  denotes the cost of taking action  $a$  in state  $s$  and the cost of a trajectory is defined as the sum of discounted costs:  $C(\tau) = \sum_{t=0}^{T-1} \gamma^t C(s_t, a_t)$ . The goal of constrained reinforcement learning is defined as to find the policy which maximizes the expected sum of discounted rewards while the expected sum of discounted costs is smaller than the budget:

$$\max_{\pi} \mathbb{E}_{\tau \sim \pi} R(\tau) \quad \text{s.t.} \quad \mathbb{E}_{\tau \sim \pi} C(\tau) < \alpha. \quad (1)$$

When  $\alpha$  is 0, constraints can be interpreted as hard constraints meaning the resulting policy should never visit states which incur any cost. When  $\alpha > 0$ , the resulting policy is allowed to obtain cost  $> 0$  in some cases, i.e. soft constraints.

### 2.2. Inverse Reinforcement Learning

Inverse Reinforcement Learning (IRL) is a learning problem which, given an expert data distribution  $\mathcal{D}$  represented by a finite set of trajectories, tries to identify the reward function  $R(s, a)$  the expert agent is optimizing. Assume the unknown reward function is defined as  $R'(s, a) = \omega \cdot \phi(s, a)$  with  $\omega \in \mathbb{R}^k$  a  $k$ -dimensional vector of real numbers and  $\phi : \mathcal{S} \times \mathcal{A} \mapsto \mathbb{R}_+^k$  denoting a fixed mapping from the state-action space to a  $k$ -dimensional vector of non-negative features. We define the feature representation of a trajectory as the sum of discounted feature vectors:  $\phi(\tau) = \sum_{t=0}^{T-1} \gamma^t \phi(s_t, a_t)$ . With forward RL we can obtain a policy which maximizes  $R'$  (i.e. the nominal policy). The problem of IRL can then be rephrased as finding values of  $\omega$  such that the expected features when following the nominal policy match the expected features under the expert data distribution, i.e. feature expectation matching (Abbeel & Ng, 2004). However, this is an ill-posed problem as many assignments of  $\omega$  will result in matching expected features. To resolve this ambiguity, Ziebart et al. (2010) proposed to choose from all values  $\omega$  which result in matching feature expectation those that maximize the causal entropy, i.e.

Maximum Causal Entropy Inverse Reinforcement Learning (MCE-IRL). Under Markovian dynamics the causal entropy of a trajectory is defined as the discounted sum of the conditional entropy of the current action given the current state:  $H(\tau) = \sum_{t=0}^{T-1} \gamma^t H(a_t | s_t)$ . Although the original feature matching objective only considers reward functions that are linear in  $\phi$ , state-of-the-art methods are scalable to complex problems by parameterizing  $R'$  with a deep neural network (Wulfmeier et al., 2015; Ho & Ermon, 2016). For an elaborate introduction to MCE-IRL we refer the reader to the work of Gleave & Toyer (2022).

### 3. Maximum Causal Entropy Inverse Constrained Reinforcement Learning

Inverse Constrained Reinforcement Learning (ICRL) methods try to learn a cost function which represents the constraints applicable to a particular environment from demonstrations of agents abiding these constraints. Inspired by the principle of maximum causal entropy (Ziebart et al., 2010) and feature expectation matching (Abbeel & Ng, 2004), we propose a novel objective for ICRL. We adopt the IRL terminology and will refer to constraint-abiding agents as expert agents.

#### 3.1. Objective

Given an expert data distribution  $\mathcal{D}$  and a reward function  $R$ , we define the primal problem as finding the stochastic policy  $\pi(a | s)$  (i.e. the nominal policy) which maximizes the given reward signal and the causal entropy while matching feature expectations between the nominal policy and the expert data distribution:

$$\begin{aligned} \max_{\pi \in \Pi} \quad & \mathbb{E}_{\tau \sim \pi} [R(\tau) + \beta H(\tau)] \quad \text{s.t.} \\ & \mathbb{E}_{\tau \sim \mathcal{D}} [\phi(\tau)] - \mathbb{E}_{\tau \sim \pi} [\phi(\tau)] \leq \alpha. \end{aligned} \quad (2)$$

Where  $\Pi$  denotes the set of normalized policies with non-negative probabilities for all states and actions:

$$\begin{aligned} \pi \in \Pi \quad & \Leftrightarrow \quad \pi(a | s) \geq 0 \\ & \text{and} \quad \int \pi(a | s) da = 1 \quad (\forall s \in \mathcal{S}). \end{aligned} \quad (3)$$

We define the entropy coefficient  $\beta$  to balance the reward and the entropy objective. The feature matching constraint is defined as an inequality constraint with a budget  $\alpha$ . To solve the constrained optimization problem in eq. (2), we define the Lagrangian and calculate its saddle points by solving the dual problem. The Lagrangian of this primal problem is found by replacing the feature matching constraint by a weighted penalty term with weights  $\lambda \in \mathbb{R}^k : \lambda_i \geq 0$  for  $0, \dots, k-1$  (i.e. dual variable vector). The Karush-Kuhn-Tucker (KKT) conditions state that for any pair of

---

#### Algorithm 1 MCE-ICRL algorithm

---

**Input:** reward function  $R(s, a)$ , expert demonstrations  $\mathcal{D}$

**Output:** cost function  $C$ , nominal policy  $\pi$

**Parameter:** number of iterations  $\eta$

---

- 1: Initialize  $\theta$ ,  $\lambda$  and  $\zeta$
  - 2: Learn nominal policy  $\pi_\theta^0$  with zero cost
  - 3: Pre-train  $\phi_\zeta$  using  $\tau \sim \pi_\theta^0$  and  $\tau \sim \mathcal{D}$  (Sec. 3.5)
  - 4: **for**  $i \leftarrow 0$  **to**  $\eta$  **do**
  - 5:   Learn  $\pi_\theta$  maximizing eq. (4) w.r.t. to the policy parameters  $\theta$  (Sec. 3.2 and 3.4).
  - 6:   Perform gradient descent on  $\lambda$  and  $\zeta$  minimizing eq. (4) w.r.t.  $\lambda$  (Sec. 3.3) and  $\zeta$  (Sec. 3.5).
  - 7: **end for**
- 

optimal points  $(\pi, \lambda)$ , all values of  $\lambda$  should be non-negative (Sec. 5.5.3 Boyd et al. (2004)). The Lagrangian of the primal problem (eq. 2) can be written as:

$$\begin{aligned} \mathcal{L}(\pi, \lambda) = & \mathbb{E}_{\tau \sim \pi} [R(\tau) + \beta H(\tau)] \\ & + \lambda \cdot (\mathbb{E}_{\tau \sim \mathcal{D}} [\phi(\tau)] - \mathbb{E}_{\tau \sim \pi} [\phi(\tau)] - \alpha). \end{aligned} \quad (4)$$

Then the dual problem can be defined as

$$\min_{\lambda} \max_{\pi \in \Pi} \mathcal{L}(\pi, \lambda). \quad (5)$$

We solve the dual problem by first maximizing the Lagrangian with respect to the policy  $\pi$  and then taking a single gradient step minimizing the Lagrangian with respect to the dual variable vector  $\lambda$  (i.e. dual ascent).

**Theorem 3.1.** *The dual problem can be solved by alternately optimizing for  $\pi$  and  $\lambda$ . When the policy update is performed on a faster time-scale than the updates on the dual variable vector,  $\pi$  and  $\lambda$  will converge to a local optimum.*

*Proof.* Chapter 6 of (Borkar, 2009).

We first discuss optimizing eq. (4) w.r.t. the policy  $\pi$  (Sec. 3.2) and then optimizing the dual variables  $\lambda$  (Sec. 3.3). Next, in Sec. 3.4 we present an approximation for the method presented in Sec. 3.2. Finally, we extend our method to non-linear cost functions (Sec. 3.5). Algorithm 1 provides an overview of the different steps of the proposed method.

#### 3.2. Policy Iteration

Maximizing the Lagrangian w.r.t. the policy corresponds with solving a planning problem. We derive a policy iteration algorithm which alternates between a policy evaluation and a policy improvement step. We will show that this algorithm converges to the optimal policy (Theorem 3.3).

**Lemma 3.2.** *The optimal policy  $\pi^*$  maximizing eq. (4) is given by*

$$\pi^*(a_t | s_t) = \exp \left( \frac{1}{\beta} (Q^*(s_t, a_t) - V^*(s_t)) \right). \quad (6)$$

With the action-value function defined by

$$Q(s_t, a_t) = R(s_t, a_t) - \lambda \cdot \phi(s_t, a_t) + \gamma \mathbb{E}_p [V(s_{t+1})], \quad (7)$$

and the state-value function by

$$V(s_t) = \beta \log \int \exp \left( \frac{1}{\beta} Q(s_t, a_t) \right) da. \quad (8)$$

*Proof.* See Section A.1 in the appendix.

The Q-function in eq. 7 resembles the Q-function of the standard entropy-regularized RL objective (Haarnoja et al., 2017) with an additional term that subtracts  $\lambda \cdot \phi(s, a)$  from the reward. In the policy evaluation step, our goal is to compute the action-value function for an arbitrary policy  $\pi$ . We can obtain the Q-function, for a fixed policy, by iteratively applying a modified Bellman backup operator  $\mathcal{T}^\pi$  given by

$$\mathcal{T}^\pi Q(s_t, a_t) \triangleq R(s_t, a_t) - \lambda \cdot \phi(s_t, a_t) + \gamma \mathbb{E}_p [V(s_{t+1})], \quad (9)$$

with  $V(s) = \mathbb{E}_\pi [Q(s, a) - \beta \log \pi(a | s)]$  (derived from eq. (6)). During the policy improvement step, we update the policy for each state towards the optimal policy (eq. (6)) using the computed Q-function according to

$$\pi_{\text{new}} = \arg \min_{\pi' \in \Pi} D_{\text{KL}} \left( \pi'(\cdot | s_t) \parallel \pi_{\text{old}}^* \right). \quad (10)$$

**Theorem 3.3 (Policy Iteration).** *Continually applying policy evaluation (using eq. (9)) and policy improvement (using eq. (10)) starting from any  $\pi \in \Pi$ , converges to the optimal policy  $\pi^*$  for which  $Q^{\pi^*}(s_t, a_t) \geq Q^\pi(s_t, a_t)$  for all  $\pi \in \Pi$  and  $(s_t, a_t) \in \mathcal{S} \times \mathcal{A}$ , assuming  $|\mathcal{A}| < \infty$ .*

*Proof.* See Section A.2 in the appendix.

### 3.3. Optimizing the Dual Variables

**Lemma 3.4.** *The Lagrange dual problem (eq. (5)) is a convex optimization problem.*

*Proof.* See Section A.3 in the appendix.

Because of lemma 3.4, the dual variables will converge to a global minimum when optimizing using gradient descent. Then, theorem 3.1 and 3.3 and lemma 3.4 prove convergence for algorithm 1 in the tabular setting.

The step we need to take on the dual variable vector is obtained by taking the gradient of the Lagrangian with respect to  $\lambda$ :

$$\nabla_\lambda \mathcal{L}(\theta, \lambda) = \mathbb{E}_{\tau \sim \mathcal{D}} [\phi(\tau)] - \mathbb{E}_{\tau \sim \pi_\theta} [\phi(\tau)] - \alpha. \quad (11)$$

After each update, negative values of  $\lambda$  are clamped to zero since all values of  $\lambda$  should be non-negative. Feature expectations under the nominal policy are calculated by

iterating over a set of trajectories sampled from the learned policy. To get the feature expectations under the expert policy we iterate over the set of given expert trajectories. Intuitively, when interpreting  $\lambda \cdot \phi(s, a)$  as a cost function in eq (7), we update  $\lambda$  such that features which occur in trajectories sampled from the nominal policy and not in the expert data result in a higher cost.

### 3.4. Policy Gradient

The algorithm presented in Sec. 3.2 only considers a tabular setting with a limited state-action space. Because of this, we present a practical algorithm which scales to continuous state-action spaces. We parameterize the policy with a neural network with parameters  $\theta$ . To recover the optimal policy, we learn the optimal parameters using a policy gradient algorithm.

**Lemma 3.5.** *Suppose that the policy  $\pi_\theta$  is differentiable with respect to its parameters  $\theta$ . Then*

$$\nabla_\theta \mathcal{L}(\theta, \lambda) = \mathbb{E}_{\tau \sim \pi_\theta} \left[ \sum_{t=0}^{T-1} \nabla_\theta \log \pi_\theta(a_t | s_t) \left( Q(s_t, a_t) - \beta \log \pi_\theta(a_t | s_t) - \sum_{t'=t}^{T-1} \gamma^{t'-t} \beta \right) \right]. \quad (12)$$

*Proof.* See Section A.4 in the appendix.

The gradient in eq. (12) resembles the standard policy gradient (Williams, 1992), with the difference that a term  $-\beta \log \pi_\theta(a_t | s_t) - \sum_{t'=t}^{T-1} \gamma^{t'-t} \beta$  was added to the action-value function. The vanilla policy gradient is characterized by no bias but high variance. Variance can be reduced while keeping bias low, by introducing a state-dependent baseline (Williams, 1992).

**Lemma 3.6.** *In the gradient of the Lagrangian (eq. (12)), we can replace  $\sum_{t'=t}^{T-1} \gamma^{t'-t} \beta$  with a state dependent baseline  $b(s_t)$ .*

*Proof.* See Section A.5 in the appendix.

Because of lemma 3.6 we can replace  $\sum_{t'=t}^{T-1} \gamma^{t'-t} \beta$  with the state-value function  $V^{\pi_\theta}(s_t)$  which is a commonly used baseline. The gradient can then be written as

$$\begin{aligned} \nabla_\theta \mathcal{L}(\theta, \lambda) &= \mathbb{E}_{\tau \sim \pi_\theta} \left[ \sum_{t=0}^{T-1} \nabla_\theta \log \pi_\theta(a_t | s_t) \right. \\ &\quad \left. \left( Q^{\pi_\theta}(s_t, a_t) - \beta \log \pi_\theta(a_t | s_t) - V^{\pi_\theta}(s_t) \right) \right] \\ &= \mathbb{E}_{\tau \sim \pi_\theta} \left[ \sum_{t=0}^{T-1} \nabla_\theta \log \pi_\theta(a_t | s_t) A^{\pi_\theta}(s_t, a_t) \right] \end{aligned} \quad (13)$$

with  $A^{\pi_\theta}(s, a)$  the advantage function. We adopt generalized advantage estimation (GAE) (Schulman et al., 2015) to obtain an approximation of the advantage.

### 3.5. Non-Linear Cost Functions

We defined the cost function as the dot product of the transposed Lagrange multiplier  $\lambda$  and the feature representation  $\phi(s, a)$ . This means we can only learn cost functions which are linear with respect to  $\phi$ . In order to learn non-linear cost functions, we replace the hard-coded feature representation with a neural network with parameters  $\zeta$ . We treat  $\zeta$  as one of the dual variables and thus update them together with  $\lambda$ . To do this we derive the gradient of the Lagrangian w.r.t.  $\zeta$ :

$$\nabla_{\zeta} \mathcal{L}(\theta, \lambda, \zeta) = \lambda \cdot (\mathbb{E}_{\tau \sim \mathcal{D}} [\nabla_{\zeta} \phi_{\zeta}(\tau)] - \mathbb{E}_{\tau \sim \pi_{\theta}} [\nabla_{\zeta} \phi_{\zeta}(\tau)]). \quad (14)$$

The outputs of  $\phi_{\zeta}$  are passed through a sigmoid activation function to assure positive feature values.

We obtained better results by pre-training the feature encoder network  $\phi_{\zeta}$ . To do this, we define a feature decoder network and train the encoder and decoder as an autoencoder trying to minimize the reconstruction error between the original data (i.e. encoder input) and the reconstruction (i.e. decoder output). The autoencoder is trained on nominal and expert data.

## 4. Experiments

We validated our approach on a gridworld environment and the ICRL benchmark proposed by Liu et al. (2022), which comprises 5 robotic domains and a realistic traffic environment. Expert trajectories are sampled from a policy trained using reward constrained policy optimization (Tessler et al., 2018) given ground truth constraints. We calculate the nominal policy using Proximal Policy Optimization (PPO) (Schulman et al., 2017). We also perform a study on the transferability of the learned cost function to other agents, an ablation study on the pre-training of the feature encoder and the influence of the hyperparameter  $\beta$ . An overview of the used hyperparameters and other details about the experiments are presented in appendix B. We compare our method, which we denote by MCE-ICRL, with three baseline methods:

- **Generative Adversarial Constraint Learning (GACL):** This method is based on the well-established imitation learning method: generative adversarial imitation learning (GAIL) (Ho & Ermon, 2016). Following Malik et al. (2021), GAIL can be adopted for ICRL by training the discriminator  $D(s, a)$  to assign 0’s to constrained state-action pairs and 1’s to valid ones. During the forward step, the policy is trained by maximizing  $\bar{r}(s, a) = r(s, a) + \log D(s, a)$ .
- **Maximum Entropy Inverse Constrained Reinforcement Learning (ME-ICRL) (Malik et al., 2021):** This method adopts the principle of maximum entropy

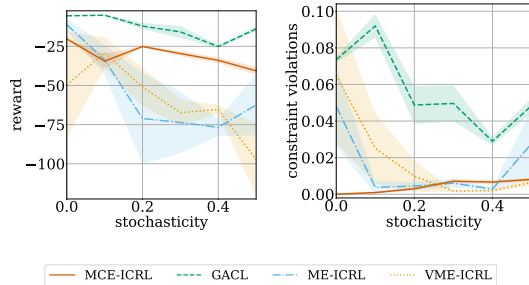


Figure 1. Evaluation of the different methods in the gridworld environment for increasing stochasticity: reward (left) and constraint violation rate (right) of trajectories sampled from the nominal policy after training. Results are averaged over 5 random seeds. The x-axis corresponds with the stochasticity. The shaded regions correspond to the standard error.

(Ziebart et al., 2008) for modeling the probability of trajectories.

- **Variational Maximum Entropy Inverse Constrained Reinforcement Learning (VME-ICRL) (Liu et al., 2022):** This method also builds on the principle of maximum entropy but models constraints as a  $\beta$ -distribution.

We evaluate the nominal policy at different points during training by sampling trajectories from it and reporting the average obtained reward and the average constraint violation rate. The reward denotes the total reward an agent has received during a trajectory. When a constraint is violated the trajectory is terminated immediately (only during evaluation). The constraint violation rate is the fraction of all timesteps of a trajectory that violate at least one constraint.

### 4.1. Gridworld

We designed a gridworld environment where the agent’s goal is to travel from a fixed initial location to a fixed goal location while avoiding constrained locations. A screenshot of this environment is shown in Sec. C in the appendix (Figure 5). Every step the agent receives a reward of  $-1$  except when it reaches the goal state, the agent gets a reward of 1. Each episode lasts a maximum of 200 timesteps. We use this environment to examine the influence of stochastic environment dynamics on the performance of learning a cost function and retrieving the optimal policy. With a particular probability, the environment ignores the action taken by the agent and instead transitions it to a randomly chosen neighboring cell. We call this probability the stochasticity of the environment. Figure 1 shows the obtained reward and constraint violations at test time for increasing stochasticity. We observed a small decrease of reward and small increase of constraint violations for MCE-ICRL for increasing stochasticity. Non-causal entropy approximates causal entropy for

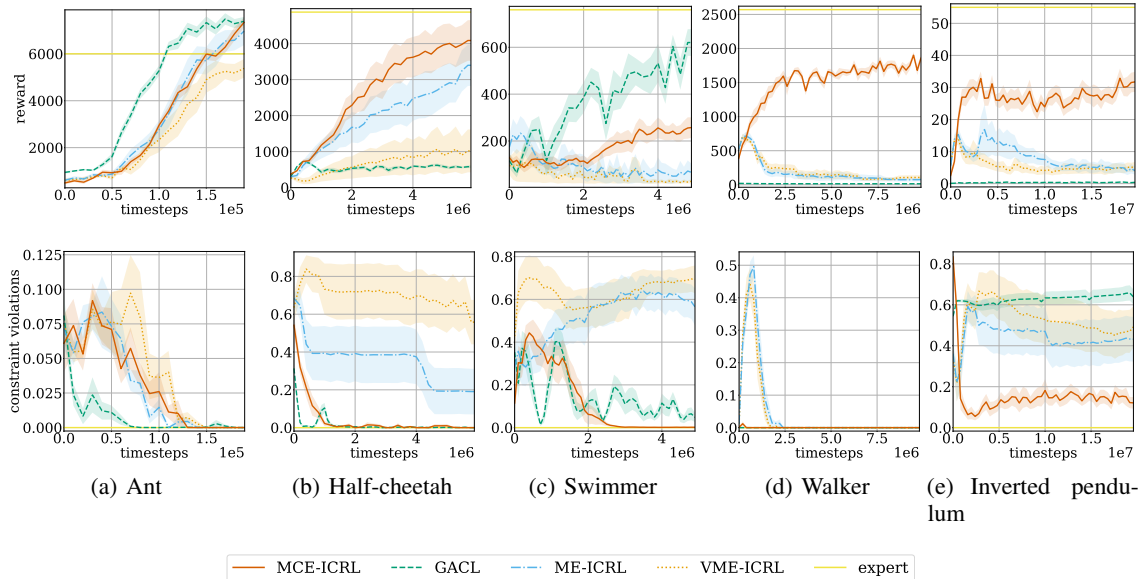


Figure 2. Evaluation of the different methods in the virtual robotics environments: reward (top) and constraint violation rate (bottom) of trajectories sampled from the nominal policy during training. Results are averaged over 10 random seeds. The x-axis is the number of timesteps taken in the environment during training. The shaded regions correspond with the standard error.

small stochasticity rates but fails when the randomness increases, this is reflected in the results of ME-ICRL and VME-ICRL. GACL receives always the largest rewards but also at the highest cost because this method was unable to learn a policy which takes the constraints into account. This supports our claim that IRL methods are not suitable for learning constraints. In Sec. D.1 of the appendix, we report extended results of experiments in the gridworld environment.

## 4.2. Virtual Robotics Environments

The virtual robotic environments are based on the MuJoCo environments from OpenAI Gym (Brockman et al., 2016) but augmented with constraints as proposed by Malik et al. (2021) and extended by Liu et al. (2022). We evaluate on five simulated robots: ant, half-cheetah, swimmer and inverted pendulum. Figure 6 (Sec. C.2 in the appendix) depicts a screenshot of each environment. This environment is characterized by a continuous state-action space and deterministic dynamics. The reward of the ant agent is proportional to the distance traveled from the starting position. The reward of the half-cheetah, swimmer and walker agents is determined by the distance it moves each step. Because of their morphology, each of these agent can move “easier” in one direction than in all other directions, but the ground truth constraints invalidate moving in the “easy” direction. The agent controlling the inverted pendulum receives higher rewards when it is to the left of the starting position. However, the ground truth cost function assigns high costs to these high reward locations. The agent should learn to bal-

ance the pendulum to the right from the origin receiving lower rewards but also lower costs. Results are depicted in figure 2. In the ant environment MCE-ICRL performs comparable to the other methods. In the half-cheetah, walker and inverted pendulum domain our method results in higher rewards and less constraint violations. In the swimmer environment MCE-ICRL results in the lowest cost and higher rewards than ME-ICRL and VME-ICRL. GACL obtains higher rewards but with more constraint violations. For every task, we also plot the reward and constraint violation rate obtained during the expert trajectories. Note there is often still a gap between the performance of the learning agent and the expert.

## 4.3. Realistic Traffic Environment

The realistic traffic environment comprises a highway driving task. This task was proposed by Liu et al. (2022) and is part of their proposed benchmark. This environment is constructed from the highD dataset (Krajewski et al., 2018) which is a dataset of naturalistic trajectories of vehicles on German highways. A scenario and an ego agent are randomly selected from the dataset for control and CommonRoad-RL (Wang et al., 2021) is used to get a state description of the ego car and its surroundings. This environment is characterized by a continuous state-action space and stochastic dynamics as the behavior of other agents in the environment is unpredictable and different expert agents act differently based on their preferences. The goal of the agent is to reach its destination at the end of the highway. Figure 7 (Sec. C.3 in the appendix) visualizes the environment. The

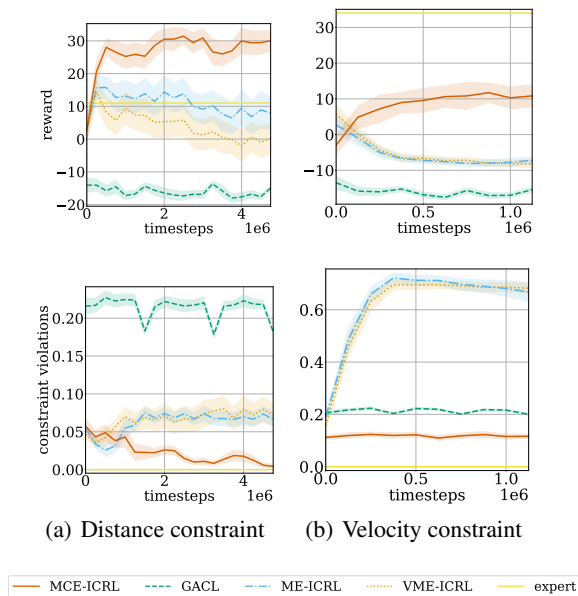


Figure 3. Evaluation of the different methods in the realistic traffic environment: reward (top) and constraint violation rate (bottom) of trajectories sampled from the nominal policy during training. Results are averaged over 10 random seeds. The x-axis is the number of timesteps taken in the environment during training. The shaded regions correspond with the standard error.

environment contains two scenarios, one with a minimum distance constraint between the ego car and other vehicles and one with a maximum velocity constraint. The results are depicted in Figure 3. Our method outperforms the other methods by a large margin which is not surprising as the traffic domain is characterized by high stochasticity. The ground truth constraints were arbitrarily chosen by Liu et al. (2022) and are in some cases violated in the starting state of the ego agent. Because of this, no method, even not the expert agent trained given the ground truth constraints, is able to reduce the cost to zero.

#### 4.4. Transfer Learning

When a cost function is learned for a specific agent, it could be beneficial when that cost function can be transferred to other types of agents operating in the same environment. This would prevent us from learning a cost function for every kind of agent. Note that constraints are often environment specific and apply to different types of agents, e.g. traffic rules apply to all vehicles on the road. To this end, we assess the transferability of a learned cost function to other types of agents which possibly have other morphologies and reward functions. We perform the transfer learning experiments proposed by Malik et al. (2021). The cost function learned for the ant agent is transferred to a “broken ant” agent for which two of its legs are disabled. We also trans-

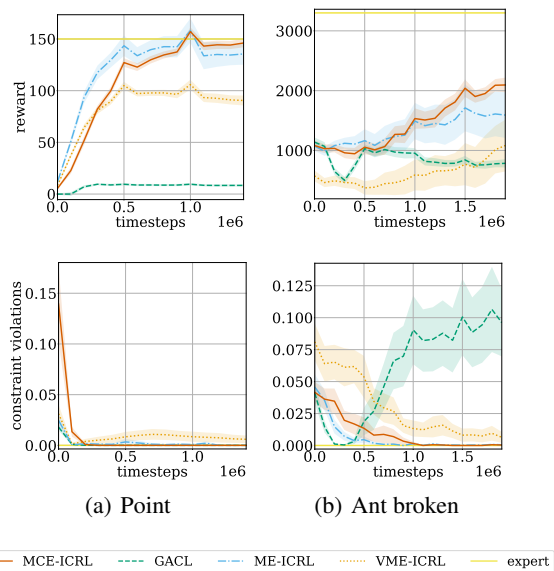


Figure 4. Evaluation of the transferability of the cost function obtained by the different methods: reward (top) and constraint violation rate (bottom) of trajectories sampled from the nominal policy during training. Results are averaged over 10 random seeds. The x-axis is the number of timesteps taken in the environment during training. The shaded regions correspond with the standard error.

fer this cost function to the point agent from OpenAI Gym (Brockman et al., 2016). The reward function of the point robot encourages the agent to move in counter clockwise in a circle at a distance of 10 units from its initial location. We adopt reward constrained policy optimization (Tessler et al., 2018) to train agents on the given reward function and the transferred cost function. The results are depicted in Figure 4. For both agents our method performs slightly better than ME-ICRL and outperforms VME-ICRL and GACL by a large margin in both reward and number of constraint violations.

#### 4.5. Ablation Studies

##### 4.5.1. INFLUENCE OF THE HYPERPARAMETER $\beta$

The entropy coefficient  $\beta$  can be interpreted as a regularization coefficient by enforcing randomness into the learned policy  $\pi$ . Table 1 reports the reward and the constraint violation rate of trajectories sampled from a policy learned using MCE-ICRL during testing for the virtual robotic environments. It is self-evident, that a policy which is more random will result in smaller rewards since the policy will be less optimal. However, when  $\beta$  reaches a certain limit, the performance starts to decrease which could be attributed to the agent overfitting on the expert trajectories.

Table 1. Ablation study on the pre-training of the feature encoder and the entropy coefficient  $\beta$ , the table contains for every agent the received reward and the constraint violation rate at test time  $\pm$  standard error, averaged over 10 random seeds and 10 trajectories per seed.

		Ant	Half-cheetah	Swimmer	Walker	Inverted pendulum
Reward	$\beta = 1e-5$	5985 $\pm$ 259	3895 $\pm$ 295	177 $\pm$ 52	1647 $\pm$ 100	27 $\pm$ 3
	$\beta = 1e-4$	<b>7338<math>\pm</math>211</b>	<b>4085<math>\pm</math>565</b>	<b>257<math>\pm</math>44</b>	<b>1858<math>\pm</math>44</b>	26 $\pm$ 3
	$\beta = 1e-3$	6057 $\pm$ 313	3499 $\pm$ 492	253 $\pm$ 54	1746 $\pm$ 81	<b>32<math>\pm</math>3</b>
	$\beta = 1e-2$	6228 $\pm$ 316	2377 $\pm$ 631	192 $\pm$ 43	1732 $\pm$ 77	29 $\pm$ 4
	no pre-training	7131 $\pm$ 313	3609 $\pm$ 490	165 $\pm$ 59	1656 $\pm$ 71	21 $\pm$ 1
Constraint violation rate	$\beta = 1e-5$	<b>0<math>\pm</math>0</b>	<b>0<math>\pm</math>0</b>	0.33 $\pm$ 0.09	<b>0<math>\pm</math>0</b>	0.22 $\pm$ 0.05
	$\beta = 1e-4$	<b>0<math>\pm</math>0</b>	<b>0<math>\pm</math>0</b>	<b>0.002<math>\pm</math>0.001</b>	<b>0<math>\pm</math>0</b>	<b>0.11<math>\pm</math>0.03</b>
	$\beta = 1e-3$	<b>0<math>\pm</math>0</b>	0.002 $\pm$ 0.002	0.12 $\pm$ 0.04	<b>0<math>\pm</math>0</b>	.12 $\pm$ 0.03
	$\beta = 1e-2$	<b>0<math>\pm</math>0</b>	0.024 $\pm$ 0.012	0.11 $\pm$ 0.05	<b>0<math>\pm</math>0</b>	0.17 $\pm$ 0.02
	no pre-training	<b>0<math>\pm</math>0</b>	<b>0<math>\pm</math>0</b>	0.22 $\pm$ 0.09	<b>0<math>\pm</math>0</b>	0.23 $\pm$ 0.04

#### 4.5.2. PRE-TRAINING THE FEATURE ENCODER

To assess the importance of pre-training the feature encoder, we train a version of MCE-ICRL without pre-training. Table 1 reports the received reward and constraint violation rate of the nominal policy at test time for the virtual robotic environments. From these results it is clear that pre-training the feature encoder provides a significant increase of the received reward. Section D in the appendix provides additional results on the effect of pre-training the feature encoder and  $\beta$  during training and for the other environments.

## 5. Related Work

### 5.1. Maximum Entropy RL

In Maximum Entropy RL (MaxEnt RL), the standard maximum reward objective is augmented with a maximum entropy objective (Ziebart et al., 2008; Toussaint, 2009; Fox et al., 2015). This augmentation has several advantages, such as improved exploration by acquiring diverse behaviours (Haarnoja et al., 2017) and better convergence and computational properties (Gu et al., 2016). Ziebart et al. (2010) extended the principle of maximum entropy to settings where information is revealed over time, i.e. principle of maximum causal entropy. This extension enables applicability in problems with partial observability, feedback and stochastic influences of the environment.

### 5.2. Learning From Experts

A variety of methods have leveraged human expertise to improve the performance of autonomous agents. Behavioral cloning uses expert demonstrations to learn a policy using supervised learning (Bain & Sammut, 1995; Ross et al., 2011). Although simple and efficient in some applications, it is possible there will be a mismatch between the training and testing state distribution which could cause a considerable decrease in performance. In preference learning, the

goal is to learn a mapping between inputs and a ranking of the inputs which represents the user’s (or expert’s) preferences (Chu & Ghahramani, 2005; Lee et al., 2021). For humans, it is often easier to provide preferences instead of complete demonstrations although the latter contains more information. Most closely related to ICRL is IRL which has the goal of learning and subsequently optimizing a reward function (Abbeel & Ng, 2004; Ho & Ermon, 2016). But as stated in the introduction and confirmed in the experiment section, IRL cannot be applied for learning constraints. We refer to the introduction for a review on ICRL literature.

## 6. Conclusion and Future Work

We proposed a novel ICRL method which is able to learn constraints in environments with stochastic dynamics. We provide a theoretical proof of convergence in a tabular setting. Next, we presented an approximation which enables our method to scale to complex problems with a continuous state-action space. Our method outperforms the state-of-the-art ICRL methods and the learned cost functions can be successfully transferred to other types of agents with different reward functions. The empirical evaluation shows that our method still does not meet the performance of expert agents in many scenarios, leaving room for improvement. The ablation study highlights the importance of a well-chosen value for  $\beta$ , and automatically tuning this parameter as proposed by Haarnoja et al. (2018) could be a valuable extension to our method. Another interesting direction is to learn constraints in an offline fashion, i.e. when no nominal model of the environment is available. Current benchmark domains only consider relatively simple constraints, often specified as location constraints. Future work is required to develop challenging benchmarks considering more complex constraints, e.g. constraints based on the state of multiple objects.



## References

- Abbeel, P. and Ng, A. Y. Apprenticeship learning via inverse reinforcement learning. In *Proceedings of the twenty-first international conference on Machine learning*, pp. 1, 2004.
- Altman, E. *Constrained Markov decision processes: stochastic modeling*. Routledge, 1999.
- Bain, M. and Sammut, C. A framework for behavioural cloning. In *Machine Intelligence 15*, pp. 103–129, 1995.
- Balakrishnan, A., Bouneffouf, D., Mattei, N., and Rossi, F. Incorporating behavioral constraints in online ai systems. In *Proceedings of the AAAI Conference on Artificial Intelligence*, volume 33, pp. 3–11, 2019.
- Bhatnagar, S. and Lakshmanan, K. An online actor–critic algorithm with function approximation for constrained markov decision processes. *Journal of Optimization Theory and Applications*, 153(3):688–708, 2012.
- Borkar, V. S. *Stochastic approximation: a dynamical systems viewpoint*, volume 48. Springer, 2009.
- Boyd, S., Boyd, S. P., and Vandenberghe, L. *Convex optimization*. Cambridge university press, 2004.
- Brockman, G., Cheung, V., Pettersson, L., Schneider, J., Schulman, J., Tang, J., and Zaremba, W. Openai gym. *arXiv preprint arXiv:1606.01540*, 2016.
- Christian, B. *The alignment problem: Machine learning and human values*. WW Norton & Company, 2020.
- Chu, W. and Ghahramani, Z. Preference learning with gaussian processes. In *Proceedings of the 22nd international conference on Machine learning*, pp. 137–144, 2005.
- Finn, C., Levine, S., and Abbeel, P. Guided cost learning: Deep inverse optimal control via policy optimization. In *International conference on machine learning*, pp. 49–58. PMLR, 2016.
- Fox, R., Pakman, A., and Tishby, N. Taming the noise in reinforcement learning via soft updates. *arXiv preprint arXiv:1512.08562*, 2015.
- Fu, J., Luo, K., and Levine, S. Learning robust rewards with adversarial inverse reinforcement learning. *arXiv preprint arXiv:1710.11248*, 2017.
- Glazier, A., Loreggia, A., Mattei, N., Rahgooy, T., Rossi, F., and Venable, B. Learning behavioral soft constraints from demonstrations, 2022. URL <https://arxiv.org/abs/2202.10407>.
- Gleave, A. and Toyer, S. A primer on maximum causal entropy inverse reinforcement learning. *arXiv preprint arXiv:2203.11409*, 2022.
- Gu, S., Lillicrap, T., Ghahramani, Z., Turner, R. E., and Levine, S. Q-prop: Sample-efficient policy gradient with an off-policy critic. *arXiv preprint arXiv:1611.02247*, 2016.
- Haarnoja, T., Tang, H., Abbeel, P., and Levine, S. Reinforcement learning with deep energy-based policies. In *International conference on machine learning*, pp. 1352–1361. PMLR, 2017.
- Haarnoja, T., Zhou, A., Abbeel, P., and Levine, S. Soft actor-critic: Off-policy maximum entropy deep reinforcement learning with a stochastic actor. In *International conference on machine learning*, pp. 1861–1870. PMLR, 2018.
- Ho, J. and Ermon, S. Generative adversarial imitation learning. *Advances in neural information processing systems*, 29, 2016.
- Kingma, D. P. and Ba, J. Adam: A method for stochastic optimization. *arXiv preprint arXiv:1412.6980*, 2014.
- Krajewski, R., Bock, J., Kloeker, L., and Eckstein, L. The highd dataset: A drone dataset of naturalistic vehicle trajectories on german highways for validation of highly automated driving systems. In *2018 21st International Conference on Intelligent Transportation Systems (ITSC)*, pp. 2118–2125, 2018. doi: 10.1109/ITSC.2018.8569552.
- Lee, K., Smith, L., Dragan, A., and Abbeel, P. B-pref: Benchmarking preference-based reinforcement learning. *arXiv preprint arXiv:2111.03026*, 2021.
- Liu, G., Luo, Y., Gaurav, A., Rezaee, K., and Poupart, P. Benchmarking constraint inference in inverse reinforcement learning. *arXiv preprint arXiv:2206.09670*, 2022.
- Malik, S., Anwar, U., Aghasi, A., and Ahmed, A. Inverse constrained reinforcement learning. In *International Conference on Machine Learning*, pp. 7390–7399. PMLR, 2021.
- Mania, H., Guy, A., and Recht, B. Simple random search provides a competitive approach to reinforcement learning. *arXiv preprint arXiv:1803.07055*, 2018.
- McPherson, D. L., Stocking, K. C., and Sastry, S. S. Maximum likelihood constraint inference from stochastic demonstrations. In *2021 IEEE Conference on Control Technology and Applications (CCTA)*, pp. 1208–1213. IEEE, 2021.

- Papadimitriou, D., Anwar, U., and Brown, D. S. Bayesian inverse constrained reinforcement learning. In *Workshop on Safe and Robust Control of Uncertain Systems (NeurIPS)*, 2021.
- Ross, S., Gordon, G., and Bagnell, D. A reduction of imitation learning and structured prediction to no-regret online learning. In *Proceedings of the fourteenth international conference on artificial intelligence and statistics*, pp. 627–635. JMLR Workshop and Conference Proceedings, 2011.
- Russell, S. *Human compatible: Artificial intelligence and the problem of control*. Penguin, 2019.
- Schulman, J., Moritz, P., Levine, S., Jordan, M., and Abbeel, P. High-dimensional continuous control using generalized advantage estimation. *arXiv preprint arXiv:1506.02438*, 2015.
- Schulman, J., Wolski, F., Dhariwal, P., Radford, A., and Klimov, O. Proximal policy optimization algorithms. *arXiv preprint arXiv:1707.06347*, 2017.
- Scobee, D. R. and Sastry, S. S. Maximum likelihood constraint inference for inverse reinforcement learning. *arXiv preprint arXiv:1909.05477*, 2019.
- Stocking, K. C., McPherson, D. L., Matthew, R. P., and Tomlin, C. J. Discretizing dynamics for maximum likelihood constraint inference, 2021. URL <https://arxiv.org/abs/2109.04874>.
- Sutton, R. S. and Barto, A. G. *Reinforcement learning: An introduction*. MIT press, Cambridge, 2018.
- Tessler, C., Mankowitz, D. J., and Mannor, S. Reward constrained policy optimization. *arXiv preprint arXiv:1805.11074*, 2018.
- Toussaint, M. Robot trajectory optimization using approximate inference. In *Proceedings of the 26th annual international conference on machine learning*, pp. 1049–1056, 2009.
- Van Moffaert, K. and Nowé, A. Multi-objective reinforcement learning using sets of pareto dominating policies. *The Journal of Machine Learning Research*, 15(1):3483–3512, 2014.
- Wang, X., Krasowski, H., and Althoff, M. Commonroad-rl: A configurable reinforcement learning environment for motion planning of autonomous vehicles. In *IEEE International Conference on Intelligent Transportation Systems (ITSC)*, 2021. doi: 10.1109/ITSC48978.2021.9564898.
- Williams, R. J. Simple statistical gradient-following algorithms for connectionist reinforcement learning. *Machine learning*, 8(3):229–256, 1992.
- Wulfmeier, M., Ondruska, P., and Posner, I. Maximum entropy deep inverse reinforcement learning. *arXiv preprint arXiv:1507.04888*, 2015.
- Ziebart, B. D., Maas, A. L., Bagnell, J. A., Dey, A. K., et al. Maximum entropy inverse reinforcement learning. In *Aaai*, volume 8, pp. 1433–1438. Chicago, IL, USA, 2008.
- Ziebart, B. D., Bagnell, J. A., and Dey, A. K. Modeling interaction via the principle of maximum causal entropy. In *ICML*, 2010.

## A. Proofs

### A.1. Lemma 3.2

The primal objective is defined as

$$\max_{\pi \in \Pi} \mathcal{L}(\pi, \lambda) \quad (15)$$

with  $\mathcal{L}(\pi, \lambda)$  the Lagrangian defined in eq. (4), and thus the optimal policy

$$\pi^* = \arg \max_{\pi \in \Pi} \mathcal{L}(\pi, \lambda). \quad (16)$$

The simplex  $\Pi$  which restricts the valid policies is defined by two constraints (see eq. (3)). The first constraint requires that  $\pi(a | s)$  is positive for all states and timesteps. We treat this constraint as implicit since the causal entropy is not defined for negative probabilities. The second constraint requires that  $\pi$  is normalized over all actions for all states and timesteps. We assume, for now, the state-action space is discrete. Augmenting the normalization constraint on the current objective gives us:

$$\begin{aligned} \pi^* &= \arg \max_{\pi \in \Pi} \mathcal{L}(\pi, \lambda) \\ \text{s.t. } &\sum_{t=0}^{T-1} \sum_{s_t \in \mathcal{S}} \left( \sum_{a \in \mathcal{A}} \pi(a | s_t) - 1 \right) = 0. \end{aligned} \quad (17)$$

Then, the Lagrangian of the optimization problem in eq. (17) is defined as

$$\Psi(\pi, \lambda, \mu) = \mathcal{L}(\pi, \lambda) + \sum_{t=0}^{T-1} \sum_{s_t \in \mathcal{S}} \mu_{s_t} \left( \sum_{a \in \mathcal{A}} \pi(a | s) - 1 \right) \quad (18)$$

with  $\{\mu_{s_t}\}_{s_t \in \mathcal{S}, 0 \leq t \leq T-1}$  the dual variables for the normalization constraint. Then the optimal policy is

$$\pi^* = \arg \max_{\pi} \Psi(\pi, \lambda, \mu). \quad (19)$$

The optimal policy  $\pi^*$  satisfies the KKT condition:

$$\nabla_{\pi} \Psi(\pi^*, \lambda, \mu) = 0. \quad (20)$$

To obtain an expression for the optimal policy, we take the gradient of the Lagrangian w.r.t. the policy, equate  $\nabla_{\pi} \Psi(\pi, \lambda, \mu)$  to zero and solve for  $\pi$ .

**Lemma A.1.** *The gradient of the Lagrangian (eq. (18)) w.r.t. to the policy  $\pi(a_t | s_t)$  is given by*

$$\begin{aligned} \nabla_{\pi(a_t | s_t)} \Psi(\pi, \lambda, \mu) &= \mu_{s_t} + \rho_{\pi}(s_t) \left( R(s_t, a_t) - \lambda \cdot \phi(s_t, a_t) - \beta \log \pi(a_t | s_t) - \beta \right. \\ &\quad \left. + \mathbb{E}_{\pi} \left[ \sum_{t'=t+1}^{T-1} \gamma^{t'-t} (R(S_{t'}, A_{t'}) - \lambda \cdot \phi(S_{t'}, A_{t'}) - \beta \log \pi(A_{t'} | S_{t'})) \middle| s_t, a_t \right] \right). \end{aligned} \quad (21)$$

*Proof.* We take the gradient of each term of the Lagrangian (eq. (18)) w.r.t. to the policy  $\pi(a_t | s_t)$  separately. Uppercase

characters  $S_t, A_t$  represent random variables while lower case characters  $s_t, a_t$  denote individual observations.

$$\nabla_{\pi(a_t|s_t)} \mathbb{E}_{\pi} [R(\tau)] \quad (22)$$

$$= \nabla_{\pi(a_t|s_t)} \mathbb{E}_{\pi} \left[ \sum_{t'=0}^{T-1} \gamma^{t'} R(S_{t'}, A_{t'}) \right] \quad (23)$$

$$= \mathbb{E}_{S_t \sim \pi} \left[ \nabla_{\pi(a_t|s_t)} \mathbb{E}_{\pi} \left[ \sum_{t'=0}^{T-1} \gamma^{t'} R(S_{t'}, A_{t'}) \middle| S_t \right] \right] \quad (24)$$

$$= \mathbb{E}_{S_t \sim \pi} \left[ \gamma^t \mathbb{I}[S_t = s_t] \nabla_{\pi(a_t|s_t)} \mathbb{E}_{\pi} \left[ \sum_{t'=t}^{T-1} \gamma^{t'-t} R(S_{t'}, A_{t'}) \middle| S_t = s_t \right] \right] \quad (25)$$

$$= \rho_{\pi}(s_t) \nabla_{\pi(a_t|s_t)} \mathbb{E}_{\pi} \left[ \sum_{t'=t}^{T-1} \gamma^{t'-t} R(S_{t'}, A_{t'}) \middle| S_t = s_t \right] \quad (26)$$

$$= \rho_{\pi}(s_t) \nabla_{\pi(a_t|s_t)} \left( \pi(a_t | s_t) \mathbb{E}_{\pi} \left[ \sum_{t'=t}^{T-1} \gamma^{t'-t} R(S_{t'}, A_{t'}) \middle| S_t = s_t, A_t = a_t \right] \right. \\ \left. + \left( \sum_{a'_t \neq a_t} \pi(a'_t | s_t) \right) \mathbb{E}_{\pi} \left[ \sum_{t'=t}^{T-1} \gamma^{t'-t} R(S_{t'}, A_{t'}) \middle| S_t = s_t, A_t \neq a_t \right] \right) \quad (27)$$

$$= \rho_{\pi}(s_t) \mathbb{E}_{\pi} \left[ \sum_{t'=t}^{T-1} \gamma^{t'-t} R(S_{t'}, A_{t'}) \middle| S_t = s_t, A_t = a_t \right] \quad (28)$$

$$= \rho_{\pi}(s_t) \left[ R(s_t, a_t) + \mathbb{E}_{\pi} \left[ \sum_{t'=t+1}^{T-1} \gamma^{t'-t} R(S_{t'}, A_{t'}) \middle| s_t, a_t \right] \right], \quad (29)$$

where  $\rho_{\pi}(s_t)$  represents the discounted probability that an agent acting according to policy  $\pi$  will be in state  $s_t$  at time  $t$

$$\rho_{\pi}(s_t) = \mathbb{E}_{S_t \sim \pi} [\gamma^t \mathbb{I}[S_t = s_t]]. \quad (30)$$

The gradient of the entropy term:

$$\nabla_{\pi(a_t|s_t)} \mathbb{E}_{\pi} [H(\tau)] \quad (31)$$

$$= \nabla_{\pi(a_t|s_t)} \mathbb{E}_{\pi} \left[ \sum_{t'=0}^{T-1} \gamma^{t'} H(A_{t'} | S_{t'}) \right] \quad (32)$$

$$= -\nabla_{\pi(a_t|s_t)} \mathbb{E}_{\pi} \left[ \sum_{t'=0}^{T-1} \gamma^{t'} \log \pi(A_{t'} | S_{t'}) \right] \quad (33)$$

$$= -\rho_{\pi}(s_t) \nabla_{\pi(a_t|s_t)} \mathbb{E}_{\pi} \left[ \sum_{t'=t}^{T-1} \gamma^{t'-t} \log \pi(A_{t'} | S_{t'}) \middle| S_t = s_t \right] \quad (34)$$

$$= -\rho_{\pi}(s_t) \nabla_{\pi(a_t|s_t)} \mathbb{E}_{\pi} \left[ \log \pi(A_t | S_t) + \sum_{t'=t+1}^{T-1} \gamma^{t'-t} \log \pi(A_{t'} | S_{t'}) \middle| S_t = s_t \right] \quad (35)$$

$$= -\rho_{\pi}(s_t) \left( 1 + \log \pi(a_t | s_t) + \mathbb{E}_{\pi} \left[ \sum_{t'=t+1}^{T-1} \gamma^{t'-t} \log \pi(A_{t'} | S_{t'}) \middle| s_t, a_t \right] \right). \quad (36)$$

The gradient of the feature matching term:

$$\nabla_{\pi(a_t|s_t)} \lambda \cdot \left( \mathbb{E}_{\mathcal{D}} \left[ \sum_{t'=0}^{T-1} \gamma^{t'} \phi(S_{t'}, A_{t'}) \right] - \mathbb{E}_{\pi} \left[ \sum_{t'=0}^{T-1} \gamma^{t'} \phi(S_{t'}, A_{t'}) \right] \right) \quad (37)$$

$$= -\nabla_{\pi(a_t|s_t)} \lambda \cdot \mathbb{E}_{\pi} \left[ \sum_{t'=0}^{T-1} \gamma^{t'} \phi(S_{t'}, A_{t'}) \right] \quad (38)$$

$$= -\rho_{\pi}(s_t) \lambda \cdot \nabla_{\pi(a_t|s_t)} \mathbb{E}_{\pi} \left[ \sum_{t'=0}^{T-1} \gamma^{t'-t} \phi(S_{t'}, A_{t'}) \middle| S_t = s_t \right] \quad (39)$$

$$= -\rho_{\pi}(s_t) \lambda \cdot \left[ \phi(s_t, a_t) + \mathbb{E}_{\pi} \left[ \sum_{t'=t+1}^{T-1} \gamma^{t'-t} \phi(S_{t'}, A_{t'}) \middle| s_t, a_t \right] \right]. \quad (40)$$

The gradient of the normalization constraint term:

$$\nabla_{\pi(a_t|s_t)} \sum_{t=0}^{T-1} \sum_{s_t \in \mathcal{S}} \mu_{s_t} \left( \sum_{a \in \mathcal{A}} \pi(a | s) - 1 \right) \quad (41)$$

$$= \mu_{s_t}. \quad (42)$$

After re-arranging the gradient from Lemma A.1, we get an expression for the optimal policy  $\pi^*$

$$\begin{aligned} \pi^*(a_t | s_t) = \exp \left( \frac{1}{\beta} \left( R(s_t, a_t) - \lambda \cdot \phi(s_t, a_t) + \frac{\mu_{s_t}}{\rho_{\pi}(s_t)} - \beta \right. \right. \\ \left. \left. + \mathbb{E}_{\pi} \left[ \sum_{t'=t+1}^{T-1} \gamma^{t'-t} (R(S_{t'}, A_{t'}) - \lambda \cdot \phi(S_{t'}, A_{t'}) - \beta \log \pi(A_{t'} | S_{t'})) \middle| s_t, a_t \right] \right) \right). \end{aligned} \quad (43)$$

We define  $V(s_t)$  and  $Q(s_t, a_t)$  as

$$V(s_t) \triangleq \frac{-\mu_{s_t}}{\rho_{\pi}(s_t)} + \beta \quad (44)$$

$$Q(s_t, a_t) \triangleq R(s_t, a_t) - \lambda \cdot \phi(s_t, a_t) + \mathbb{E}_{\pi} \left[ \sum_{t'=t+1}^{T-1} \gamma^{t'-t} (R(S_{t'}, A_{t'}) - \lambda \cdot \phi(S_{t'}, A_{t'}) - \beta \log \pi(A_{t'} | S_{t'})) \middle| s_t, a_t \right]. \quad (45)$$

The optimal policy can then be described as

$$\pi^*(a_t | s_t) = \exp \left( \frac{1}{\beta} (Q(s_t, a_t) - V(s_t)) \right). \quad (46)$$

In eq. (3) we defined the set of valid policies as the set of normalized policies  $\Pi$  and assume all values of  $\mu$  are chosen such that  $\sum_{a \in \mathcal{A}} \pi(a | s) = 1 \forall s \in \mathcal{S}$ . Because of this, we can say that  $\forall s \in \mathcal{S}$ :

$$1 = \sum_{a \in \mathcal{A}} \pi(a | s) \quad (47)$$

$$= \sum_{a \in \mathcal{A}} \exp \left( \frac{1}{\beta} (Q(s, a) - V(s)) \right) \quad (48)$$

$$\exp \left( \frac{1}{\beta} V(s) \right) = \sum_{a \in \mathcal{A}} \exp \left( \frac{1}{\beta} (Q(s, a) - V(s)) \right) \exp \left( \frac{1}{\beta} V(s) \right) \quad (49)$$

$$= \sum_{a \in \mathcal{A}} \exp \left( \frac{1}{\beta} Q(s, a) \right) \quad (50)$$

$$V(s) = \beta \log \sum_{a \in \mathcal{A}} \exp \left( \frac{1}{\beta} Q(s, a) \right). \quad (51)$$

For a continuous action space we get

$$V(s) = \beta \log \int \exp\left(\frac{1}{\beta} Q(s, a)\right) da. \quad (52)$$

Similarly, it can be demonstrated that

$$Q(s_t, a_t) = R(s_t, a_t) - \lambda \cdot \phi(s_t, a_t) + \mathbb{E}_\pi \left[ \sum_{t'=t+1}^{T-1} \gamma^{t'-t} (R(S_{t'}, A_{t'}) - \lambda \cdot \phi(S_{t'}, A_{t'}) - \beta \log \pi(A_{t'} | S_{t'})) \middle| s_t, a_t \right] \quad (53)$$

$$= R(s_t, a_t) - \lambda \cdot \phi(s_t, a_t) + \gamma \mathbb{E}_p \left[ \mathbb{E}_\pi [Q(S_{t+1}, A_{t+1}) - \beta \log \pi(A_{t+1} | S_{t+1})] \middle| s_t, a_t \right] \quad (54)$$

$$= R(s_t, a_t) - \lambda \cdot \phi(s_t, a_t) + \gamma \mathbb{E}_p \left[ \mathbb{E}_\pi [Q(S_{t+1}, A_{t+1}) - (Q(S_{t+1}, A_{t+1}) - V(S_{t+1}))] \middle| s_t, a_t \right] \quad (55)$$

$$= R(s_t, a_t) - \lambda \cdot \phi(s_t, a_t) + \gamma \mathbb{E}_p \left[ V(S_{t+1}) \middle| s_t, a_t \right]. \quad (56)$$

### A.2. Theorem 3.3

First, we will prove the convergence of the policy evaluation step.

**Lemma A.2** (Policy Evaluation). *Starting with an initial  $Q$ -function  $Q^0 : \mathcal{S} \times \mathcal{A} \rightarrow \mathbb{R}$  with  $|\mathcal{A}| < \infty$ , where  $Q^{k+1} = \mathcal{T}^\pi Q^k$ . Then the sequence  $Q^k$  will converge to the  $Q$ -value of  $\pi$  as  $k \rightarrow \infty$ .*

*Proof.*

We define an augmented reward signal as

$$R_\pi(s_t, a_t) \triangleq R(s_t, a_t) - \lambda \cdot \phi(s_t, a_t) + \beta H(a_t | s_t). \quad (57)$$

Applying the standard convergence results for policy evaluation (Sutton & Barto, 2018) proves the lemma. It is necessary to have  $|\mathcal{A}| < \infty$  in order to ensure that the augmented reward is bounded.

For the projection presented in eq. (10), we can prove that the new, projected policy has a higher value than the old policy according to the objective in eq. (4).

**Lemma A.3** (Policy Improvement). *Given  $\pi_{old} \in \Pi$  and  $\pi_{new}$  be the policy obtained by solving the minimization problem defined in eq. (10). Then  $Q^{\pi_{new}}(s_t, a_t) \geq Q^{\pi_{old}}(s_t, a_t)$  for all  $(s_t, a_t) \in \mathcal{S} \times \mathcal{A}$  with  $|\mathcal{A}| < \infty$ .*

*Proof.*

Let  $Q^{\pi_{old}}$  and  $V^{\pi_{old}}$  be the action-value and state-value function corresponding to  $\pi_{old} \in \Pi$ . We can define  $J_{\pi_{old}}$  as

$$J_{\pi_{old}}(\pi'(\cdot | s_t)) = D_{KL} \left( \pi' \parallel \exp\left(\frac{1}{\beta} (Q^{\pi_{old}}(s_t | \cdot) - V^{\pi_{old}}(s_t))\right) \right). \quad (58)$$

Then  $\pi_{new}$  can be defined as

$$\pi_{new}(\cdot | s_t) = \arg \min_{\pi' \in \Pi} J_{\pi_{old}}(\pi'(\cdot | s_t)). \quad (59)$$

The inequality  $J_{\pi_{old}}(\pi_{new}(\cdot | s_t)) \leq J_{\pi_{old}}(\pi_{old}(\cdot | s_t))$  must hold, as we have the option of always selecting  $\pi_{new} = \pi_{old}$  from the set of policies  $\Pi$ . Hence

$$\mathbb{E}_{\pi_{new}} \left[ \log \pi_{new}(a_t | s_t) - \frac{1}{\beta} (Q^{\pi_{old}}(s_t, a_t) - V^{\pi_{old}}(s_t)) \right] \leq \mathbb{E}_{\pi_{old}} \left[ \log \pi_{old}(a_t | s_t) - \frac{1}{\beta} (Q^{\pi_{old}}(s_t, a_t) - V^{\pi_{old}}(s_t)) \right] \quad (60)$$

$$\mathbb{E}_{\pi_{new}} \left[ \log \pi_{new}(a_t | s_t) - \frac{1}{\beta} Q^{\pi_{old}}(s_t, a_t) \right] + \frac{1}{\beta} V^{\pi_{old}}(s_t) \leq \mathbb{E}_{\pi_{old}} \left[ \log \pi_{old}(a_t | s_t) - \frac{1}{\beta} Q^{\pi_{old}}(s_t, a_t) \right] + \frac{1}{\beta} V^{\pi_{old}}(s_t) \quad (61)$$

$$\mathbb{E}_{\pi_{new}} \left[ \log \pi_{new}(a_t | s_t) - \frac{1}{\beta} Q^{\pi_{old}}(s_t, a_t) \right] \leq \mathbb{E}_{\pi_{old}} \left[ \log \pi_{old}(a_t | s_t) - \frac{1}{\beta} Q^{\pi_{old}}(s_t, a_t) \right] \quad (62)$$

$$\mathbb{E}_{\pi_{new}} [Q^{\pi_{old}}(s_t, a_t) - \beta \log \pi_{new}(a_t | s_t)] \geq V^{\pi_{old}}(s_t). \quad (63)$$

We can bring  $V^{\pi_{old}}$  outside of the expectation since the state-value function only depends on the current state (line 2). The last line follows from the definition of the optimal policy in eq. (6). We can repeatedly expand the Bellman equation by applying the Bellman equation and the inequality of eq. (63):

$$Q^{\pi_{old}}(s_t, a_t) = R(s_t, a_t) - \lambda \cdot \phi(s_t, a_t) + \gamma \mathbb{E}_p [V^{\pi_{old}}(s_{t+1})] \quad (64)$$

$$\leq R(s_t, a_t) - \lambda \cdot \phi(s_t, a_t) + \gamma \mathbb{E}_{p, \pi_{new}} [Q^{\pi_{old}}(s_{t+1}, a_{t+1}) - \beta \log \pi_{new}(a_{t+1} | s_{t+1})] \quad (65)$$

$$\vdots \quad (66)$$

$$\leq Q^{\pi_{new}}(s_t, a_t). \quad (67)$$

Then, the convergence to  $Q^{\pi_{new}}$  follows from Lemma A.2.

At each iteration  $i$ , the policy  $\pi_i$  will reach an optimum due to Lemma A.3. Because the sequence  $Q^{\pi_i}$  increases monotonically and is bounded for  $\pi \in \Pi$ , the sequence converges to some  $\pi^*$ . We have to prove that  $\pi^*$  is indeed optimal. At convergence, it must be the case that  $J_{\pi^*}(\pi^*(\cdot | s_t)) < J_{\pi^*}(\pi(\cdot | s_t))$  for all  $\pi \in \Pi, \pi \neq \pi^*$ . By repeatedly expanding  $Q^{\pi^*}$  as done in Lemma A.3, we can show that  $Q^{\pi^*}(s_t, a_t) > Q^{\pi}(s_t, a_t)$  for all  $(s_t, a_t) \in \mathcal{S} \times \mathcal{A}$ . Thus, the value of any other policy in  $\Pi$  is lower than that of the converged policy. This makes  $\pi^*$  optimal in  $\Pi$ .

### A.3. Lemma 3.4

$\max_{\pi \in \Pi} \mathcal{L}(\pi, \lambda)$  can be viewed as a pointwise maximum of affine functions of  $\lambda$ , thus is concave.  $\lambda \geq 0$  is an affine constraint. Hence, the dual problem (eq. (5)) is a convex optimization problem.

### A.4. Lemma 3.5

We calculate the gradient of each term of the Lagrangian eq. (4) separately w.r.t. the policy parameters  $\theta$ . The gradient of the causal entropy term is

$$\nabla_{\theta} \mathbb{E}_{\tau \sim \pi_{\theta}} [H(\tau)] \quad (68)$$

$$= \nabla_{\theta} \mathbb{E}_{\tau \sim \pi_{\theta}} \left[ \sum_{t=0}^{T-1} \gamma^t H(a_t | s_t) \right] \quad (69)$$

$$= -\nabla_{\theta} \mathbb{E}_{\tau \sim \pi_{\theta}} \left[ \sum_{t=0}^{T-1} \gamma^t \log \pi_{\theta}(a_t | s_t) \right] \quad (70)$$

$$= -\nabla_{\theta} \sum_{\tau} \left( P(\tau | \pi_{\theta}) \sum_{t=0}^{T-1} \gamma^t \log \pi_{\theta}(a_t | s_t) \right) \quad (71)$$

$$= -\sum_{\tau} \left( \nabla_{\theta} P(\tau | \pi_{\theta}) \sum_{t=0}^{T-1} \gamma^t \log \pi_{\theta}(a_t | s_t) + P(\tau | \pi_{\theta}) \sum_{t=0}^{T-1} \gamma^t \nabla_{\theta} \log \pi_{\theta}(a_t | s_t) \right) \quad (72)$$

$$= -\sum_{\tau} \left( P(\tau | \pi_{\theta}) \nabla_{\theta} \log P(\tau | \pi_{\theta}) \sum_{t=0}^{T-1} \gamma^t \log \pi_{\theta}(a_t | s_t) + P(\tau | \pi_{\theta}) \sum_{t=0}^{T-1} \gamma^t \nabla_{\theta} \log \pi_{\theta}(a_t | s_t) \right) \quad (73)$$

$$= -\sum_{\tau} P(\tau | \pi_{\theta}) \left( \nabla_{\theta} \log P(\tau | \pi_{\theta}) \sum_{t=0}^{T-1} \gamma^t \log \pi_{\theta}(a_t | s_t) + \sum_{t=0}^{T-1} \gamma^t \nabla_{\theta} \log \pi_{\theta}(a_t | s_t) \right) \quad (74)$$

$$= -\mathbb{E}_{\tau \sim \pi_{\theta}} \left[ \nabla_{\theta} \log P(\tau | \pi_{\theta}) \sum_{t=0}^{T-1} \gamma^t \log \pi_{\theta}(a_t | s_t) + \sum_{t=0}^{T-1} \gamma^t \nabla_{\theta} \log \pi_{\theta}(a_t | s_t) \right] \quad (75)$$

$$= -\mathbb{E}_{\tau \sim \pi_{\theta}} \left[ \sum_{t=0}^{T-1} \nabla_{\theta} \log \pi_{\theta}(a_t | s_t) \sum_{t'=t}^{T-1} \gamma^{t'-t} \log \pi_{\theta}(a_{t'} | s_{t'}) + \sum_{t=0}^{T-1} \gamma^t \nabla_{\theta} \log \pi_{\theta}(a_t | s_t) \right] \quad (76)$$

$$= -\mathbb{E}_{\tau \sim \pi_{\theta}} \left[ \sum_{t=0}^{T-1} \nabla_{\theta} \log \pi_{\theta}(a_t | s_t) \left( \sum_{t'=t}^{T-1} \gamma^{t'-t} \log \pi_{\theta}(a_{t'} | s_{t'}) + 1 \right) \right]. \quad (77)$$

In line 2 and 3, we apply the definition of causal entropy.  $P(\tau | \pi)$  denotes the probability of a trajectory  $\tau$  under policy  $\pi$ . Line 6 follows from  $\nabla P(\tau | \pi) = P(\tau | \pi) \nabla \log P(\tau | \pi)$ . Line 9 follows from the definition of the probability of a trajectory  $\tau$  under a policy  $\pi$ :  $P(\tau | \pi) = \mathcal{I}(s_0) \prod_{t=0}^{T-1} p(s_{t+1} | s_t, a_t) \pi(a_t | s_t)$ . Then the second sum needs to be updated since the policy at time  $t'$  cannot affect the policy at time  $t$  when  $t < t'$  because of the causal relation between consecutive states. The gradient of the reward term can be calculated similarly

$$\nabla_{\theta} \mathbb{E}_{\tau \sim \pi_{\theta}} [R(\tau)] \quad (78)$$

$$= \mathbb{E}_{\tau \sim \pi_{\theta}} \left[ \sum_{t=0}^{T-1} \nabla_{\theta} \log \pi(a_t | s_t) \sum_{t'=t}^{T-1} \gamma^{t'-t} R(s_t, a_t) \right], \quad (79)$$

and the feature matching term:

$$\nabla_{\theta} \lambda \cdot \left( \mathbb{E}_{\tau \sim \mathcal{D}} \left[ \sum_{t=0}^{T-1} \gamma^t \phi(s_t, a_t) \right] - \mathbb{E}_{\tau \sim \pi_{\theta}} \left[ \sum_{t=0}^{T-1} \gamma^t \phi(s_t, a_t) \right] - \alpha \right) \quad (80)$$

$$= -\nabla_{\theta} \lambda \cdot \mathbb{E}_{\tau \sim \pi_{\theta}} \left[ \sum_{t=0}^{T-1} \gamma^t \phi(s_t, a_t) \right] \quad (81)$$

$$= -\mathbb{E}_{\tau \sim \pi_{\theta}} \left[ \sum_{t=0}^{T-1} \nabla_{\theta} \log \pi(a_t | s_t) \sum_{t'=t}^{T-1} \gamma^{t'-t} \lambda \cdot \phi(s_t, a_t) \right]. \quad (82)$$

In our work, the same discount factor is used to discount rewards, costs and entropies. Putting it all together, we get

$$\nabla_{\theta} \mathcal{L}(\theta, \lambda) = \mathbb{E}_{\tau \sim \pi_{\theta}} \left[ \sum_{t=0}^{T-1} \nabla_{\theta} \log \pi_{\theta}(a_t | s_t) \sum_{t'=t}^{T-1} \gamma^{t'-t} (R(s_{t'}, a_{t'}) - \lambda \cdot \phi(s_{t'}, a_{t'}) - \beta \log \pi_{\theta}(a_{t'} | s_{t'}) - \beta) \right]. \quad (83)$$

We rewrite eq. (83)

$$\begin{aligned} \nabla_{\theta} \mathcal{L}(\theta, \lambda) = & \mathbb{E}_{\tau \sim \pi_{\theta}} \left[ \sum_{t=0}^{T-1} \nabla_{\theta} \log \pi_{\theta}(a_t | s_t) \left( R(s_t, a_t) - \lambda \cdot \phi(s_t, a_t) \right. \right. \\ & \left. \left. + \sum_{t'=t+1}^{T-1} \gamma^{t'-t} (R(s_{t'}, a_{t'}) - \lambda \cdot \phi(s_{t'}, a_{t'}) - \beta \log \pi_{\theta}(a_{t'} | s_{t'})) - \beta \log \pi_{\theta}(a_t | s_t) - \sum_{t'=t}^{T-1} \gamma^{t'-t} \beta \right) \right]. \quad (84) \end{aligned}$$

Using the definition of the action-value function (eq. (7)) we obtain:

$$\nabla_{\theta} \mathcal{L}(\theta, \lambda) = \mathbb{E}_{\tau \sim \pi_{\theta}} \left[ \sum_{t=0}^{T-1} \nabla_{\theta} \log \pi_{\theta}(a_t | s_t) \left( Q(s_t, a_t) - \beta \log \pi_{\theta}(a_t | s_t) - \sum_{t'=t}^{T-1} \gamma^{t'-t} \beta \right) \right]. \quad (85)$$

### A.5. Lemma 3.6

We can replace  $\sum_{t'=t}^{T-1} \gamma^{t'-t} \beta$  with a state dependent baseline  $b(s_t)$  in eq. (12) only when this does not affect the gradient  $\nabla_{\theta} \mathcal{L}(\theta, \lambda)$ . We rewrite eq. (12):

$$\nabla_{\theta} \mathcal{L}(\theta, \lambda) = \mathbb{E}_{\tau \sim \pi_{\theta}} \left[ \sum_{t=0}^{T-1} \nabla_{\theta} \log \pi_{\theta}(a_t | s_t) \left( Q(s_t, a_t) - \beta \log \pi_{\theta}(a_t | s_t) - \sum_{t'=t}^{T-1} \gamma^{t'-t} \beta \right) \right] \quad (86)$$

$$= \mathbb{E}_{\tau \sim \pi_{\theta}} \left[ \sum_{t=0}^{T-1} \nabla_{\theta} \log \pi_{\theta}(a_t | s_t) \left( Q(s_t, a_t) - \beta \log \pi_{\theta}(a_t | s_t) \right) \right] \quad (87)$$

$$- \mathbb{E}_{\tau \sim \pi_{\theta}} \left[ \sum_{t=0}^{T-1} \nabla_{\theta} \log \pi(a_t | s_t) \sum_{t'=t}^{T-1} \gamma^{t'-t} \beta \right] \quad (88)$$



In the second term, we replace  $\sum_{t'=t}^{T-1} \gamma^{t'-t} \beta$  with a state-dependent baseline  $b(s_t)$  which gives us:

$$\nabla_{\theta} \mathcal{L}(\theta, \lambda) = \mathbb{E}_{\tau \sim \pi_{\theta}} \left[ \sum_{t=0}^{T-1} \nabla_{\theta} \log \pi_{\theta}(a_t | s_t) (Q(s_t, a_t) - \beta \log \pi_{\theta}(a_t | s_t)) \right] \quad (89)$$

$$- \mathbb{E}_{\tau \sim \pi_{\theta}} \left[ \sum_{t=0}^{T-1} \nabla_{\theta} \log \pi(a_t | s_t) b(s_t) \right] \quad (90)$$

Since the introduced baseline only affects the second term it suffices to proof that

$$\mathbb{E}_{\tau \sim \pi_{\theta}} \left[ \sum_{t=0}^{T-1} \nabla_{\theta} \log \pi(a_t | s_t) \sum_{t'=t}^{T-1} \gamma^{t'-t} \beta \right] = \mathbb{E}_{\tau \sim \pi_{\theta}} \left[ \sum_{t=0}^{T-1} \nabla_{\theta} \log \pi(a_t | s_t) b(s_t) \right] \quad (91)$$

$$\mathbb{E}_{\tau \sim \pi_{\theta}} \left[ \sum_{t=0}^{T-1} \nabla_{\theta} \log \pi_{\theta}(a_t | s_t) b(s_t) \right] \quad (92)$$

$$= \mathbb{E}_{s_{0:T-1}, a_{0:T-1}} \left[ \sum_{t=0}^{T-1} \nabla_{\theta} \log \pi_{\theta}(a_t | s_t) b(s_t) \right] \quad (93)$$

$$= \mathbb{E}_{s_{0:t}, a_{0:t-1}} \left[ \sum_{t=0}^{T-1} \mathbb{E}_{s_{t+1:T-1}, a_{t:T-1}} [\nabla_{\theta} \log \pi_{\theta}(a_t | s_t) b(s_t)] \right] \quad (94)$$

$$= \mathbb{E}_{s_{0:t}, a_{0:t-1}} \left[ \sum_{t=0}^{T-1} b(s_t) \mathbb{E}_{s_{t+1:T-1}, a_{t:T-1}} [\nabla_{\theta} \log \pi_{\theta}(a_t | s_t)] \right] \quad (95)$$

$$= \mathbb{E}_{s_{0:t}, a_{0:t-1}} \left[ \sum_{t=0}^{T-1} b(s_t) \mathbb{E}_{a_t} [\nabla_{\theta} \log \pi_{\theta}(a_t | s_t)] \right] \quad (96)$$

$$= \mathbb{E}_{s_{0:t}, a_{0:t-1}} \left[ \sum_{t=0}^{T-1} b(s_t) \sum_{a_t \in \mathcal{A}} \pi_{\theta}(a_t | s_t) \nabla_{\theta} \log \pi_{\theta}(a_t | s_t) \right] \quad (97)$$

$$= \mathbb{E}_{s_{0:t}, a_{0:t-1}} \left[ \sum_{t=0}^{T-1} b(s_t) \sum_{a_t \in \mathcal{A}} \nabla_{\theta} \pi_{\theta}(a_t | s_t) \right] \quad (98)$$

$$= \mathbb{E}_{s_{0:t}, a_{0:t-1}} \left[ \sum_{t=0}^{T-1} b(s_t) \nabla_{\theta} \sum_{a_t \in \mathcal{A}} \pi_{\theta}(a_t | s_t) \right] \quad (99)$$

$$= \mathbb{E}_{s_{0:t}, a_{0:t-1}} \left[ \sum_{t=0}^{T-1} b(s_t) \nabla_{\theta} \cdot 1 \right] \quad (100)$$

$$= 0 \quad (101)$$

$\mathbb{E}_{\tau \sim \pi_{\theta}} \left[ \sum_{t=0}^{T-1} \nabla_{\theta} \log \pi(a_t | s_t) \sum_{t'=t}^{T-1} \gamma^{t'-t} \beta \right]$  can be solved similarly and also results in 0.



### C. Details on the Environments

In this section we provide details on and screenshots from the environments used for evaluation.

#### C.1. Gridworld

Figure 5 shows the gridworld used in the experiments, with the yellow “I” representing the initial state, the yellow “O” the goal state and the red crosses the constrained states.

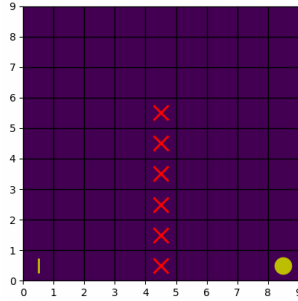


Figure 5. Gridworld environment

#### C.2. Virtual Robotics Environment

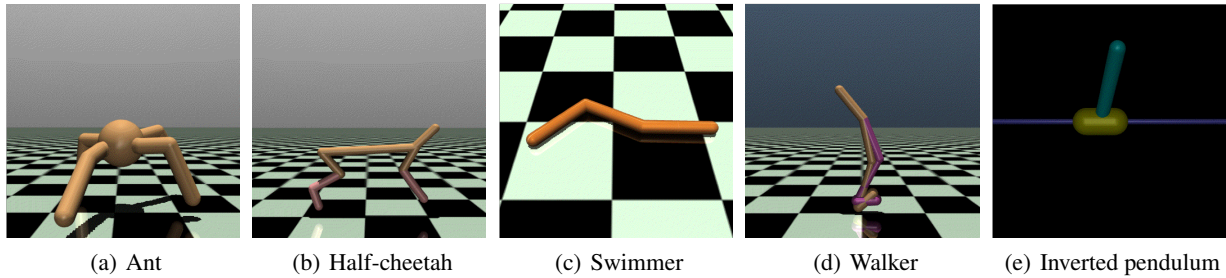


Figure 6. Screenshots from the virtual robotics environments.

#### C.3. Realistic Traffic Environment

Figure 7 shows the realistic traffic environment (image from original publication (Liu et al., 2022)). The ego car is shown in blue, other cars are red. The agent only has partial state information, observations are restricted by an observation radius (visualized in blue around the ego agent). The agent’s destination is shown in yellow.

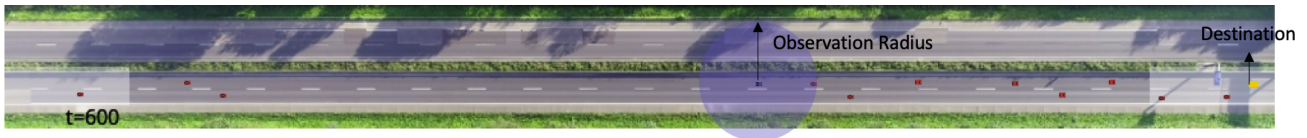


Figure 7. Realistic traffic environment

## D. More Experimental Results

### D.1. Gridworld

Figure 8(a) shows the states visited by the expert which are used as input for our method. Figure 8(b) reports the learned cost function when using MCE-ICRL with  $\beta = 0.01$ . Figure 8(c) shows the state visitations of the nominal agent.

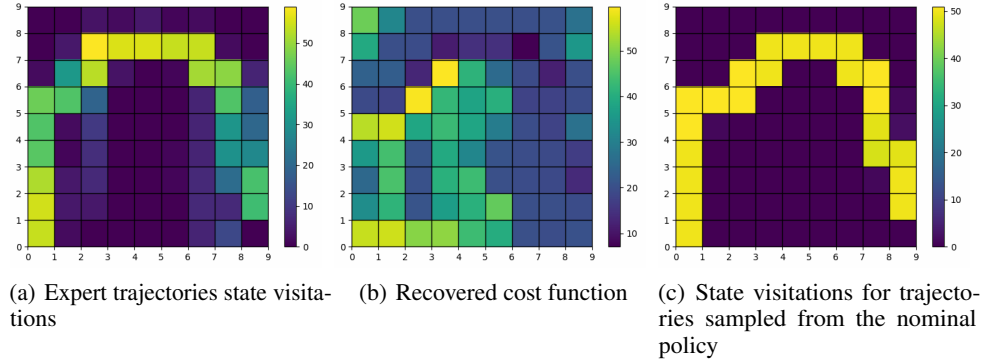


Figure 8. Results from MCE-ICRL ( $\beta = 0.01$ ) in the proposed gridworld environment.

Figure 9 depicts the reward and constraint violation rate during training at different timesteps for the different methods for different rates of stochasticity.

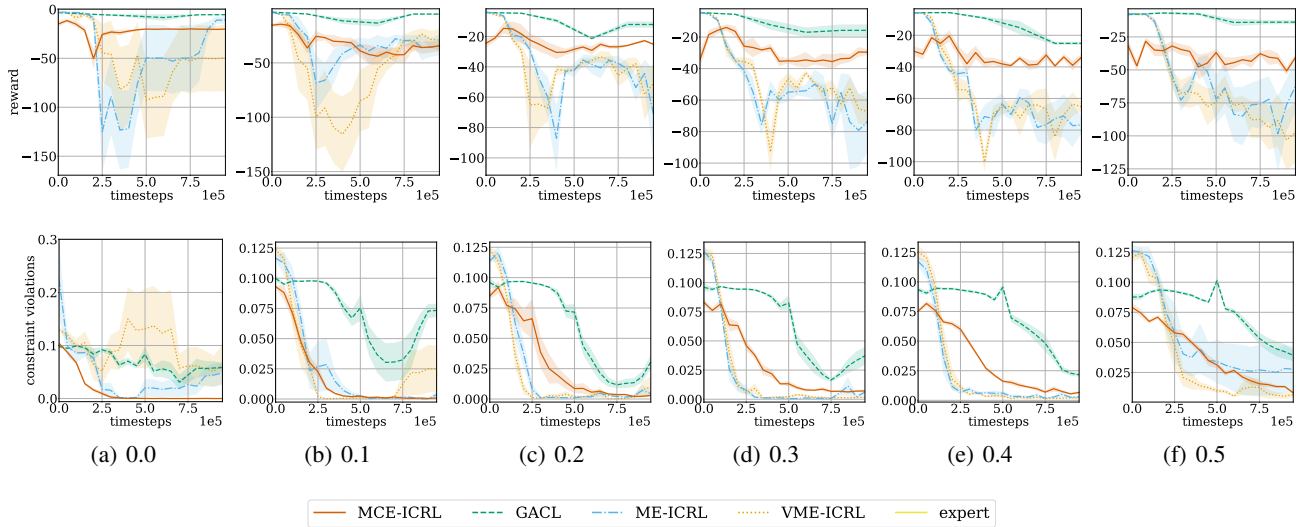


Figure 9. Evaluation of the different methods in the gridworld environment for different rates of stochasticity: reward (top) and constraint violation rate (bottom) of trajectories sampled from the nominal policy during training. Results are averaged over 5 random seeds. The x-axis is the number of timesteps taken in the environment during training. The shaded regions correspond with the standard error.

Figure 10 depicts the reward and constraint violation rate during training at different timesteps for our method with various value of  $\beta$  and for different rates of stochasticity.

Figure 11 depicts the reward received and the constraint violation rate during training for the ablation study on the pre-training of the feature encoder.

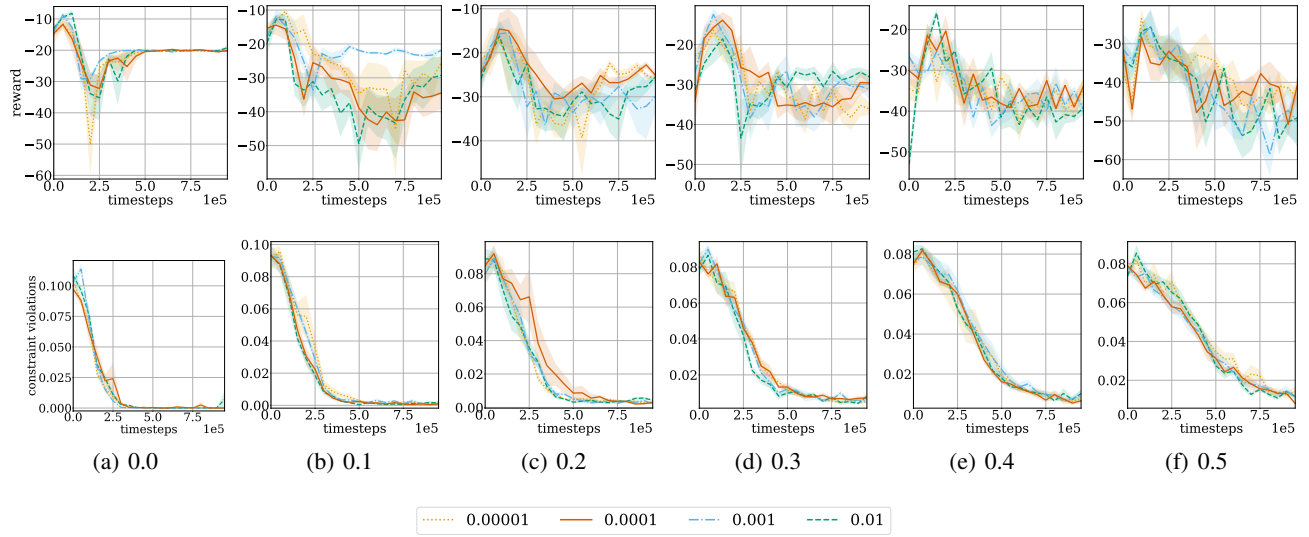


Figure 10. Evaluation of our method in the gridworld environment for different values of  $\beta$ : reward and constraint violation rate of trajectories sampled from the nominal policy during training. Results are averaged over 5 random seeds. The x-axis is the number of timesteps taken in the environment during training. The shaded regions correspond with the standard error.

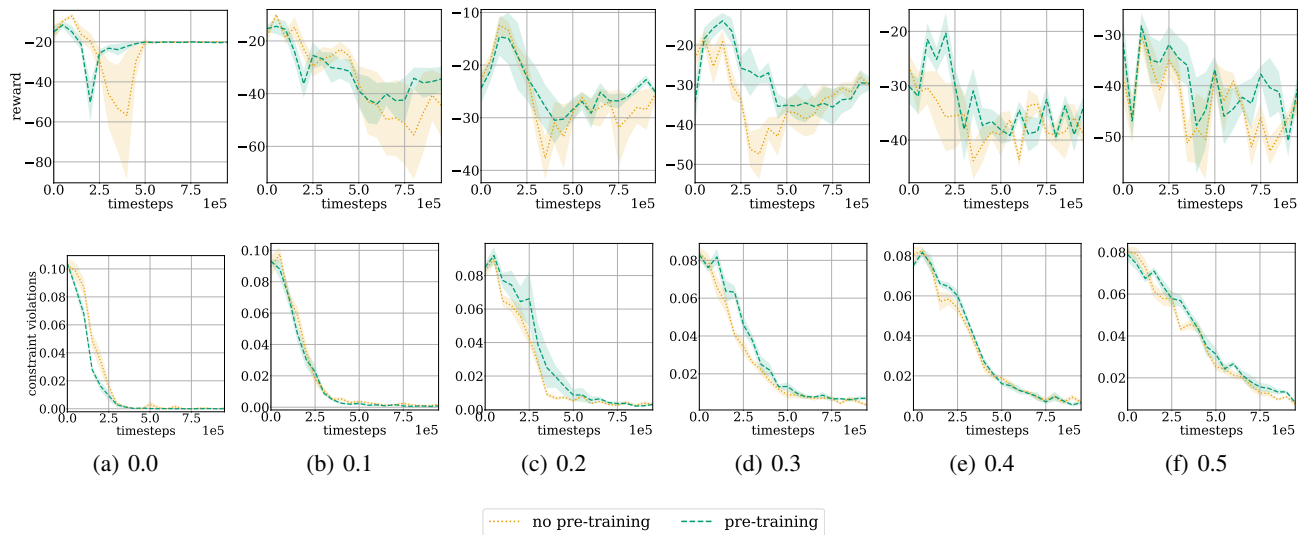


Figure 11. Evaluation of our method in the gridworld environment for feature encoder pre-training disabled: reward and constraint violation rate of trajectories sampled from the nominal policy during training. Results are averaged over 5 random seeds. The x-axis is the number of timesteps taken in the environment during training. The shaded regions correspond with the standard error.

D.2. Virtual Robotics Environments

Figure 12 depicts the reward received and the constraint violation rate during training for different values of  $\beta$ .

Figure 13 depicts the reward received and the constraint violation rate during training for the ablation study on the pre-training of the feature encoder.

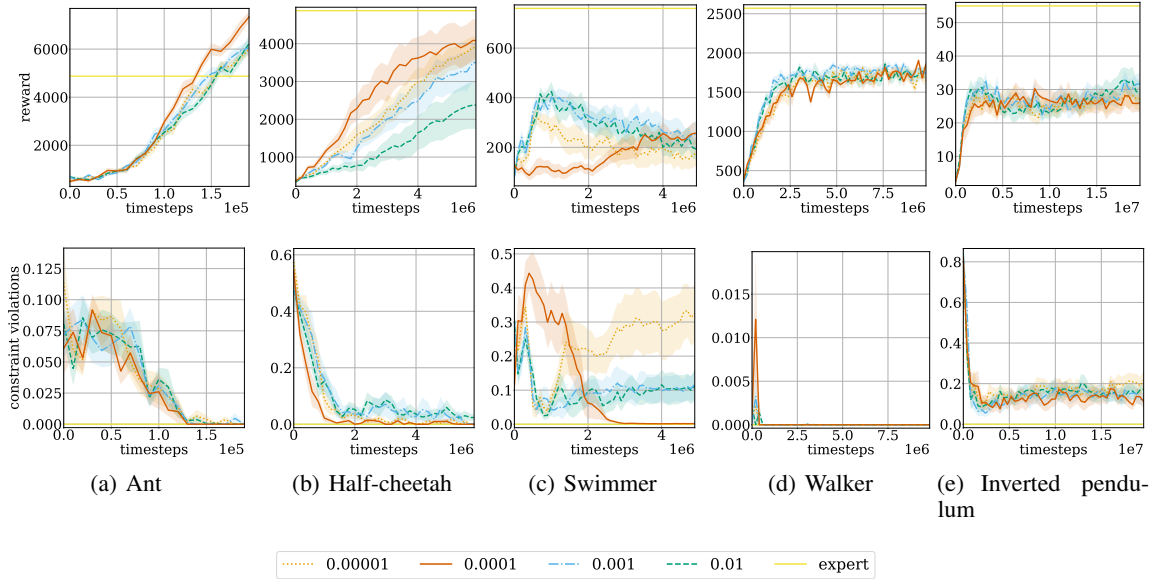


Figure 12. Evaluation of our method in the virtual robotics environments for different values of  $\beta$ : reward and constraint violation rate of trajectories sampled from the nominal policy during training. Results are averaged over 10 random seeds. The x-axis is the number of timesteps taken in the environment during training. The shaded regions correspond with the standard error.

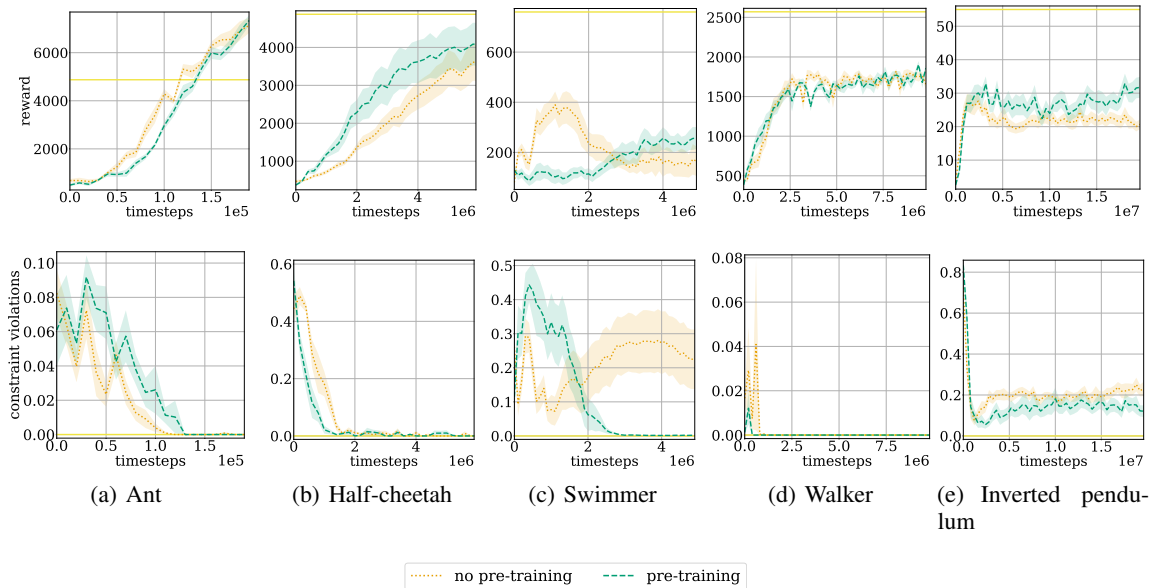


Figure 13. Evaluation of our method in the virtual robotics environments for feature encoder pre-training disabled: reward and constraint violation rate of trajectories sampled from the nominal policy during training. Results are averaged over 10 random seeds. The x-axis is the number of timesteps taken in the environment during training. The shaded regions correspond with the standard error.

D.3. Realistic Traffic Environment

Figure 14 depicts the reward and constraint violation rate during training at different timesteps for our method with various value of  $\beta$ .

Figure 15 depicts the reward received and the constraint violation rate during training for the ablation study on the pre-training of the feature encoder.

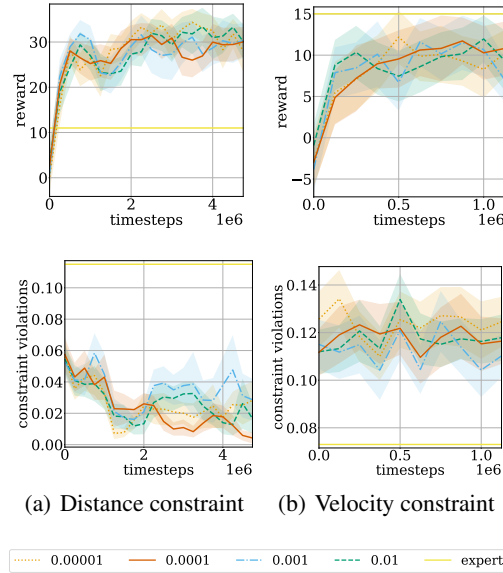


Figure 14. Evaluation of our method in the realistic traffic environment environment for different values of  $\beta$ : reward (top) and constraint violation rate (bottom) of trajectories sampled from the nominal policy during training. Results are averaged over 10 random seeds. The x-axis is the number of timesteps taken in the environment during training. The shaded regions correspond with the standard error.

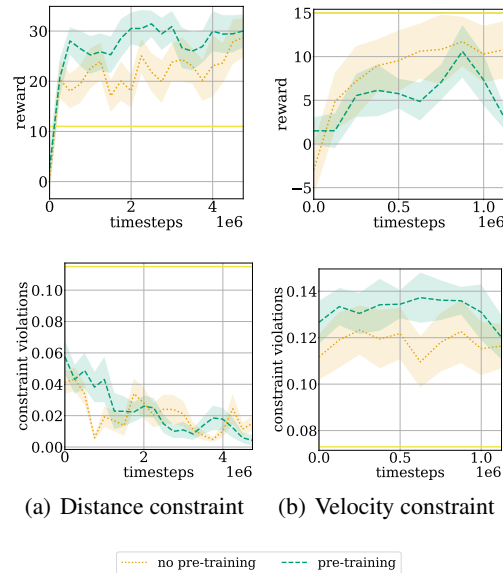


Figure 15. Evaluation of our method in the realistic traffic environment for feature encoder pre-training disabled: reward and constraint violation rate of trajectories sampled from the nominal policy during training. Results are averaged over 10 random seeds. The x-axis is the number of timesteps taken in the environment during training. The shaded regions correspond with the standard error.